THE SMALL MULTI-FUNCTION AUTONOMOUS RESEARCH AND TEACHING SONDE (SMARTSONDE): RELATING IN-SITU MEASUREMENTS OF ATMOSPHERIC PARAMETERS TO RADAR RETURNS

Phillip B. Chilson[1], **Timothy A. Bonin**[1], **Brett S. Zielke**[1], **and Sheila Kirkwood**[2]

[1]*School of Meteorology and Atmospheric Radar Research Center, University of Oklahoma, Norman, Oklahoma, USA*
[2]*Polar Atmospheric Research, Swedish Institute of Space Physics, Box 812, 98128 Kiruna, Sweden*

ABSTRACT

In-situ measurements of the atmospheric dynamic and thermodynamic state are typically obtained using instrumented towers, balloons, or piloted aircraft. An alternative to these traditional approaches is instrumented unmanned aerial systems (UAS). Here we discuss one such system: the Small Multi-function Autonomous Research and Teaching Sonde (SMARTSonde). The SMARTSonde platform is capable of directly measuring pressure, temperature, and humidity, and retrieving estimates of the horizontal wind vector. The availability of such atmospheric measurements over large spatial domains provides unquestionable value to meteorological studies. Here we discuss the design, development, and initial implementation of the SMARTSonde platform and how observations can be used to complement radar observations of the atmosphere - especially those operating near 50 MHz.

Key words: Unmanned Aerial System; Atmospheric Dynamics and Thermodynamics; Radar.

1. INTRODUCTION

In the fall of 2008, the University of Oklahoma (OU) Atmospheric Radar Research Center (ARRC) began developing a small UAS to facilitate studies of the lower atmosphere. The resulting SMARTSonde (Small Multi-function Autonomous Research and Teaching Sonde) has been designed to i) collect in-situ atmospheric measurements along either controlled or pre-configured flight paths; ii) operate autonomously; and iii) support real-time full-duplex communication (including data transfer) with a ground station [1]. Moreover, the project is intended to foster interdisciplinary student involvement at both the graduate and undergraduate levels. The concept is very similar to the SUMO (Small Unmanned Meteorological Observer) project presented in [2]. SMARTSonde is being integrated into a variety of research areas including measurements of the atmospheric boundary layer, the validation of radar-based estimates of atmospheric parameters, radar calibration, and so forth.

Meteorologists first proposed using miniature airplanes to sample the atmosphere as far back as the 1970s [3]. Efforts to accomplish this goal faltered at that time due to a lack of compact and lightweight meteorological sensors. Today, with pressure sensors smaller than a human fingernail, miniaturized temperature and humidity probes, and advances in microchip processors, the effort to create unmanned airplanes with atmospheric sensors attached has seen a resurgence. Researchers in Germany [4], Norway [2], China [5] and the United States [6] among others have begun creating miniature automated airplanes to sample the atmosphere.

Small UAS platforms offer great promise for probing the lower atmosphere. They can be deployed in remote areas with little existing infrastructure and fly into areas that may be to dangerous or difficult to access otherwise. They can also be specially designed for specific tasks. For example, [7, 8] have used UASs to measure the environment surrounding mountains including upslope and downslope flow. SMARTSonde was primarily developed to sample the planetary boundary layer but can be used to probe the lower free troposphere as well.

2. SMARTSONDE CONCEPT

Two small electric powered aircraft have been used in field operations as part of the SMARTSonde project so far: the Hobbico Nextstar (2 m wingspan, weight 4 kg) and the Multiplex Funjet (80 cm wingspan, 700 g weight shown in Figure 1). Both include a Paparrazi based autopilot system [9] with an onboard microprocessor that receives continuous readings from GPS (global position-

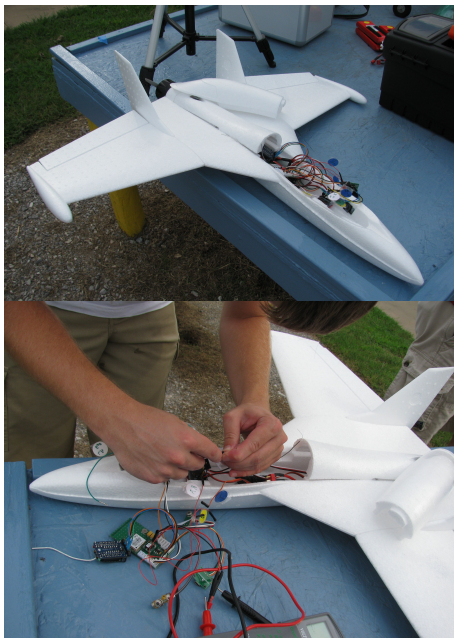

Figure 1. Pictures of one of the SMARTSonde platforms (Funjet) used in the project.

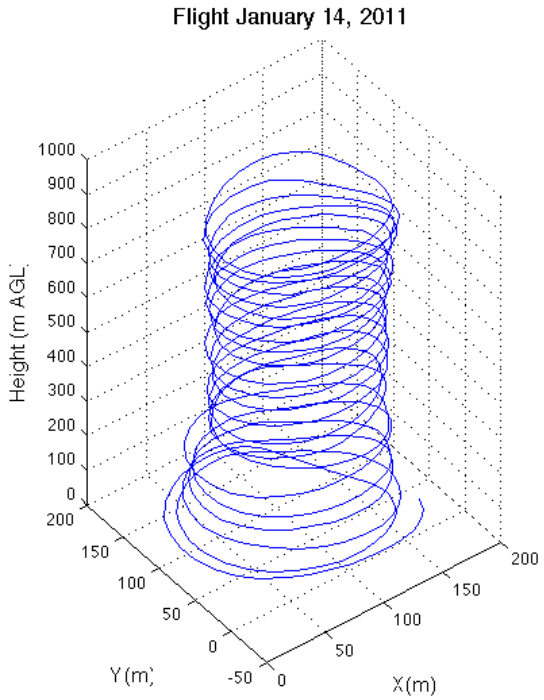

Figure 2. Example of a helical ascent pattern used during a SMARTSonde flight for the purpose of profiling the atmosphere.

ing system) and IR (infrared) detectors in order to determine the planes locations and orientations. In-situ sensors mounted on the SMARTSonde platforms directly measure pressure, temperature, and humidity. Estimates of the horizontal wind vector are retrieved from GPS and pitot tube data using specially developed wind retrieval algorithms [10]. Additionally, a sensor for measuring ozone concentrations is being developed and tested.

The SMARTSonde onboard autopilot allows flight plans to be customized to the particular phenomenon under examination. For example, conventional atmospheric profiling can be achieved by flying in a circular pattern (good spatial averaging) while maintaining a constant ascent rate (consistent vertical sampling). If one is only interested in collecting data within a certain height interval in the atmosphere then a quick ascent rate could be used to gain altitude followed by a slow helical ascent to acquire high vertical resolution sampling within the region of interest. Based on observations collected in real time, the flight plan can be modified "on the fly." Once on the ground, the time required to prepare for the next launch is only about 10 minutes.

3. SAMPLE SMARTSONDE DATA

Although still in development, several sets of observations have been successfully collected with SMARTSonde under varying meteorological conditions. Here we discuss measurements from two separate days: one corresponding to a well mixed boundary layer and the other during a morning transition of the boundary layer. Measurements on both days were performed in central Oklahoma near the OU campus.

Well Mixed Boundary Layer: Several SMARTSonde flights were completed on January 14, 2011 during conditions consistent with a well mixed afternoon boundary layer. Measurements for one of these flights collected shortly after 17:00 local time are presented in Figures 2-4. The plane performed a steady helical ascent starting near the surface and ascending up to a height of about 900 m above ground level as shown in Figure 2. Profiles of the potential temperature and specific humidity are provided in Figure 3. The potential temperature was calculated using the standard expression $\Theta = T(p/1000)^{2/7}$, where Θ is the potential temperature [K], T is the temperature [K] and p is the pressure [hPa]. Accompanying pressure data were also collected during the flights but are not shown. The wind estimates presented in Figure 4 were calculated using the technique described in [10]. Data from the other flights are similar to those shown in the figures.

Although there is nothing particularly remarkable about the measurements shown in Figures 3 and 4, they do illustrate the capabilities of SMARTSonde to effectively

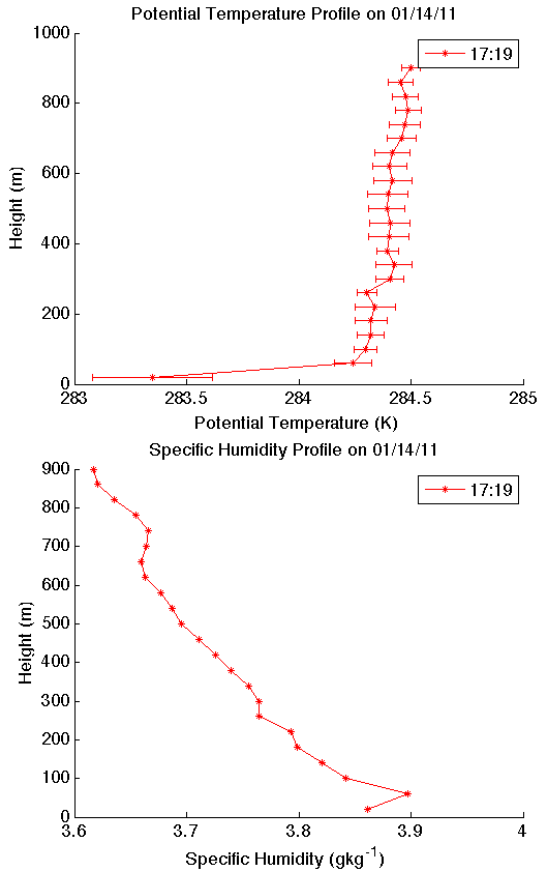

Figure 3. Profiles of potential temperature and specific humidity corresponding to the ascent shown in Figure 2.

collect dynamic and thermodynamic profiles. That is, the measurements are consistent with expectations for a well mixed boundary layer. With the exception of a shallow temperature inversion near the surface, the atmosphere is generally dry adiabatic throughout the range of observations as indicated by the constant values of Θ in Figure 3. Several comparisons between radiosonde and sodar data have also shown good agreement with measurements from the SMARTSonde platforms.

Morning Transition of the Boundary Layer: Boundary layer transitions from stable to convective and convective to stable conditions are observed in the morning and evening periods, respectively. The ability to monitor such transitions using in-situ instruments with adequate spatial and temporal resolution is challenging. SMARTSonde is well suited to these types of measurements. Data collected during a morning transition on March 6, 2011 are presented in Figures 5 and 6. Whereas the thermodynamic state of well mixed boundary layers is not expected to change dramatically over short periods of time, this is not the case for boundary layer transitions. Therefore, dynamic and thermodynamic profiles from two consecutive flights (08:25 and 08:29 local time) are shown. The first

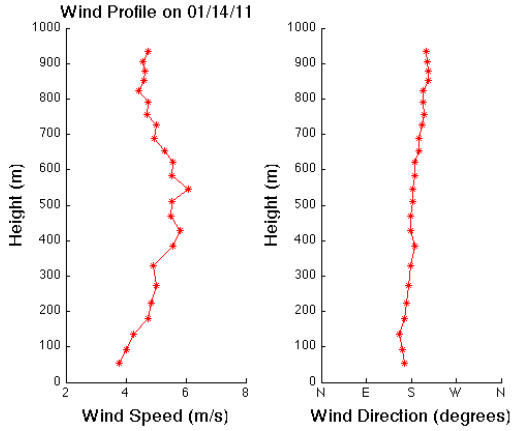

Figure 4. Retrieved profiles of the horizontal wind vector corresponding to the ascent shown in Figure 2.

profiles obtained at 08:25 are representative of a stable boundary layer with signs of initial heating in the surface layer. By 08:59, mixing is already beginning to occur and extends up to a height of 200 m above ground level. This is apparent in both the potential temperature and specific humidity.

A relatively common feature of the boundary layer in the Great Plains region of the United States is the low-level jet (LLJ) associated with the stable nocturnal conditions [11, 12]. The LLJ typically forms in the lowest 1000 to 1500 m of the atmosphere. A weak LLJ can be seen between 100 and 200 m above ground level in the wind data for 08:25 presented in Figure 6. The LLJ can also be seen in wind profiles from earlier flights on that morning (not shown). The onset of convection observed at 08:59 causes erosion of the LLJ. One of the advantages of the SMARTSonde concept is that it allows for profiling of the atmosphere with adequate temporal resolution to observe rapidly evolving atmospheric phenomena.

4. DERIVED QUANTITIES RELATED TO RADAR OBSERVATIONS

Next we examine how SMARTSonde data can complement observations from atmospheric radar. In particular, we consider wind profiling radars (wind profilers) operating near 50 MHz (VHF). Wind profilers sample the atmosphere using vertically or near vertically directed beams of radio waves and are used to detect scatter that results from gradients in the refractive index or "clear-air scatter". The gradients can occur as the result of turbulent or systematic process in the atmosphere, which ultimately determines the nature of the clear-air scatter. We will consider both mechanisms and show how data from SMARTSonde can be used to help interpret clear-air scat-

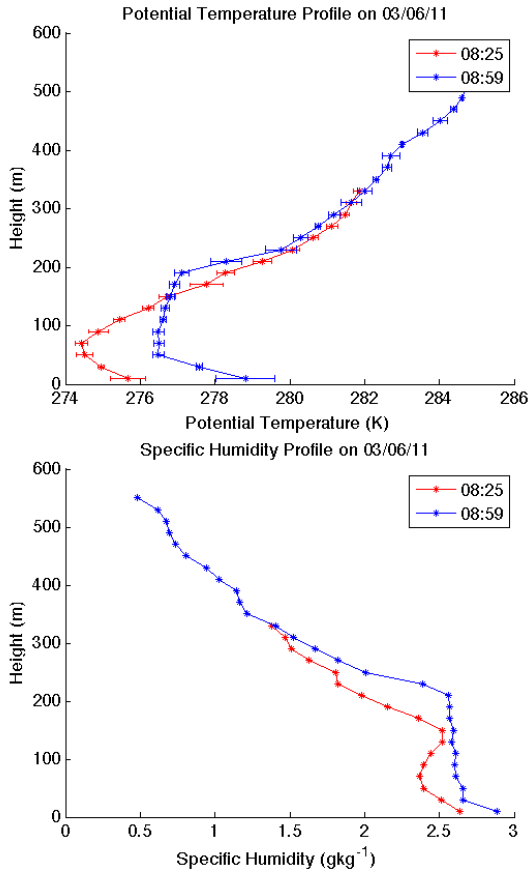

Figure 5. Profiles of potential temperature and specific humidity corresponding to a morning transition of the boundary layer.

ter. Clear-air scatter is not limited to VHF radars and wind profilers operate at other frequencies, but for the present discussion we will restrict our attention to scatter for radio waves at or near 50 MHz.

For the case of turbulent (Bragg) scatter, it has been shown that the power P_r of the returned signal measured at vertical incidence follows the relationship

$$P_r = \left(\frac{\pi P_t L_t A_e \Delta z}{64(2\ln 2)\lambda^{1/3} z^2} \right) a V_f L_0^{4/3} M^2, \qquad (1)$$

where P_t is the peak transmit power, L_t is a factor that takes losses in the antenna feed into account (less than unity), A_e is the effective area of the antenna, Δz is the range resolution, a is the ratio of eddy diffusion coefficients for potential refractive index and heat (approximately equal to unity for the cases being considered), V_f is a factor for the extent to which the sampling volume is filled with turbulence (less than or equal to unity), L_0 is the outer scale of turbulence for the inertial subrange, M is the mean vertical gradient of generalized potential refractive index, λ is the radar wavelength, and z is the distance to the scanning volume [13, 14, 15]. The terms inside the parentheses are in principle known. The mean

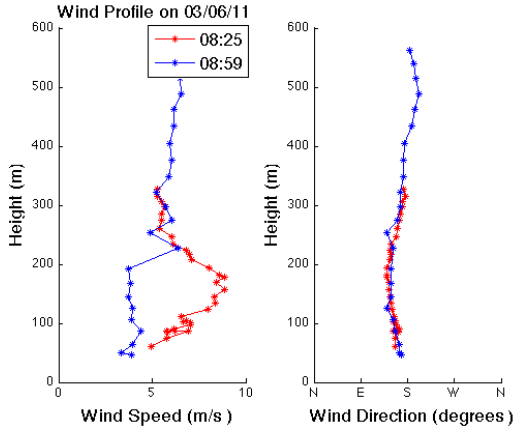

Figure 6. Profiles of the retrieved wind during a morning transition of the boundary layer. Evidence of an eroding low-level jet can be seen.

vertical gradient of generalized potential refractive index M is related to the thermodynamic conditions in the atmosphere and their vertical gradients through the equation

$$M = -77.6 \times 10^{-6} \frac{p}{T} \frac{\delta \ln \Theta}{\delta z} \left[1 + \frac{15,500q}{T} \left(1 - \frac{1}{2} \frac{\delta \ln q/\delta z}{\delta \ln \Theta/\delta z} \right) \right], \qquad (2)$$

where p is the pressure [hPa], Θ is the potential temperature [K], T is the temperature [K], and q is the specific humidity [kg kg^{-1}] [16, 17].

Next we consider the scatter from systematic or organized gradients in the refractive index which extend horizontally over lengths greater than the Fresnel radius within the radar beam. It was shown by [18] that such a condition could produce partial reflections of VHF radio waves. Moreover, the cumulative effect of having several sharp gradients located within a radar sampling volume results in Fresnel scatter. The theory of Fresnel scatter was examined by [14, 19, 20] and shown to follow

$$P_r = \left(\frac{P_t L_t A_e^2 \Delta z}{4\lambda^2 z^2} \right) F^2(\lambda) M^2, \qquad (3)$$

where $F(\lambda)$ is a function related to the fine-scale structure of the underlying vertical gradients in the refractive index at half the radar wavelength. Here again, the terms inside the parentheses are in principle known.

Both Bragg and Fresnel scatter as given by Eqs. 1 and 3, respectively, can contribute to the received backscattered power P_r observed by a vertically directed VHF radar. And both are related to the quantity M^2, which can be calculated using data from SMARTSonde. To illustrate this capability, we have calculated M^2 for the two examples presented above. Profiles of M^2 for these cases are shown in Figures 7 and 8.

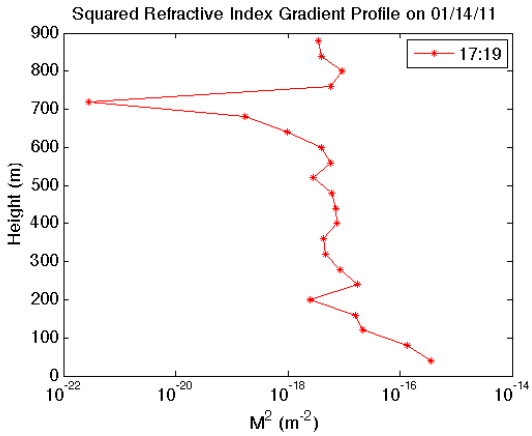

Figure 7. Retrieved profiles of M^2 for the case of the well mixed boundary layer presented in Figures 2 - 4.

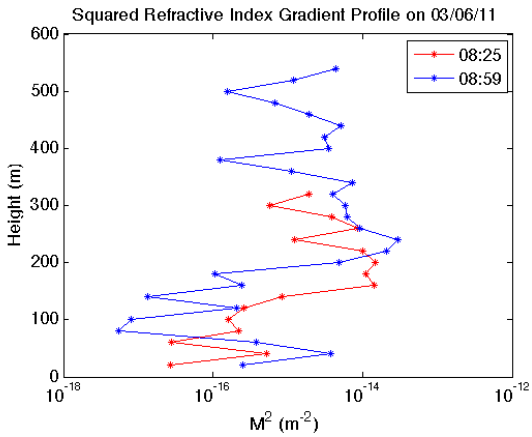

Figure 8. Retrieved profiles of M^2 for the case of the morning transition of the boundary layer presented in Figures 5 - 6.

There are numerous applications for combined VHF wind profiler and UAS observations of the atmosphere. One possible scenario in which combined observations are made is provided in Figure 9. Data collected from such an experiment could be used to calibrate the measured radar reflectivity using the procedure outlined in [21]. If the radar has been calibrated and one can determine which of the scattering mechanisms is dominant, then the recorded power from the radar in conjunction with measurements of M^2 from the UAS can be used to estimate the outer scale of turbulence L_0 (Bragg scatter) or $F^2(\lambda)$ (Fresnel scatter). For the case of Bragg scatter, it is necessary to either assume volume filling turbulence or estimate V_f using the UAS data. The extent to which VHF radio-wave scatter is aspect sensitive can be used to determine if Bragg or Fresnel scatter dominates [22, 23]. It has been stated by [23] that the preponderance of wind profiler observations in the troposphere and stratosphere at VHF can be attributed to Fresnel scatter.

Another metric that can be used to judge whether to expect Bragg or Fresnel scatter is static stability. The backscattered power received by a vertically directed VHF radar can be used to estimate the Brunt-Väisäilä frequency, which is a measure of the atmospheric static stability [15]. If contributions from atmospheric moisture can be neglected, then

$$M \approx M_D = -77.6 \times 10^{-6} \frac{p}{T} \frac{N^2}{g}, \tag{4}$$

where M_D is the dry term in the vertical gradient of generalized potential refractive index and N is the Brunt-Väisäilä frequency given by

$$N^2 = \frac{g}{\Theta} \frac{\partial \Theta}{\partial z} = g \left(\frac{\partial \ln \Theta}{\partial z} \right), \tag{5}$$

where g is the gravitational acceleration. As the degree of static stability increases, so does the value of N^2. The ratio p/T in Eq. 5 is proportional to the atmospheric density, which can be modeled using an exponential function and incorporated into a method of retrieving values of N^2 based entirely on radar observations [15]. These estimates are improved, however, if one can introduce a humidity correction.

Finally we note that SMARTSonde can be used to directly measure the structure function for n and in the case of homogeneous and isotropic turbulence measure the structure function parameter for n. The refractive index n for the neutral atmosphere is given by

$$n = 1 + 77.6 \times 10^{-6} \frac{p}{T} + 3.73 \times 10^{-1} \frac{e}{T^2}, \tag{6}$$

where e is the partial pressure of water vapor [hPa], p is the atmospheric pressure [hPa], and T is the atmospheric temperature [K] [24]. Therefore, measurements from SMARTSonde contain all parameters needed to calculate n. The structure function parameter C_n^2 can then be found through the equation

$$C_n^2 = \frac{\langle (n(r) - n(r+\Delta))^2 \rangle}{\Delta^{2/3}}, \tag{7}$$

where $n(r)$ is the refractive index at some position in space and Δ is the spatial displacement from that position r. Furthermore, Δ should fall within the inertial subrange of turbulence. The angle brackets $< \cdot >$ indicate an expectation value, which can be evaluated by allowing the airplane to repeatedly revisit the positions r and $r + \Delta$, for example by flying in a circle.

For the case of Bragg scatter, [25] discusses how the radar reflectivity η can be expressed either in terms of M^2 or C_n^2. The value of η is give by

$$\eta = \frac{a L_0^{4/3} M^2}{\lambda^{1/3}} = 3.79 \frac{C_n^2}{\lambda^{1/3}}. \tag{8}$$

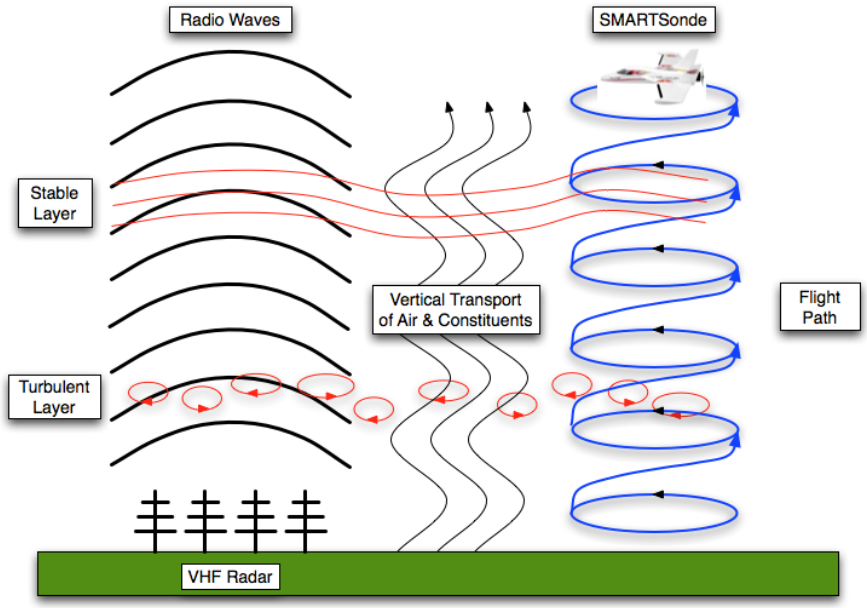

Figure 9. Depiction of combined atmospheric measurements using a VHF wind profiler and SMARTSonde. Bragg and Fresnel scatter could be associated with the stable and turbulent layers, respectively.

Therefore, if the region being probed by SMARTSonde is filled with homogeneous, isotropic turbulence and Δ falls within the inertial subrange then we can calculate C_n^2. Furthermore, if we have profiles of p, T, and q, then we can also calculate M^2. This allows us to estimate the value of L_0 using Eq. 8.

5. SUMMARY

We have provided a brief introduction to SMARTSonde and discussed the utility of making lower atmospheric measurements using such a small instrumented UAS. The SMARTSonde design resulted in part from discussions with members of the SUMO project team, which also uses a Multiplex Funjet as its airframe [2]. Over the course of several measurement campaigns, the value of SUMO has been successfully demonstrated and the Funjet has been able to obtain atmospheric profiles up to about 4 km above ground level [26, 27]. We are confident that SMARTSonde will be equally successful.

SMARTSonde can provide observations of the dynamic and thermodynamic state of the atmosphere, which are particularly valuable when validating remote sensing instruments such as radar. We have also discussed the basics of radar clear-air scatter at VHF and demonstrated how observations from SMARTSonde can be used in concert with radar data. Observations from instrumented UAS platforms such as SMARTSonde could prove crucial to developing a better understanding of VHF radar returns and how they can be used when characterizing the lower atmosphere. SMARTSonde is capable of providing detailed information in the lower atmosphere (< 4 km), which could complement conventional radiosonde data. That is, data obtained using SMARTSonde will not only allow us to assess the static and dynamic stability of the atmosphere, but also thoroughly test radar scattering theory.

6. ACKNOWLEDGEMENTS

Funding to support the development of SMARTSonde has been provided by the University of Oklahoma (OU) Atmospheric Radar Research Center (ARRC) and through a grant provided by the National Oceanic Atmospheric Administration (NOAA) National Severe Storms Laboratory (NSSL).

REFERENCES

[1] P. B. Chilson, A. M. Gleason, B. Zielke, F. Nai, M. Yeary, P. M. Klein, and W. Shalamunec. SMARTSonde: A small UAS platform to support radar research. In *Proc. AMS 34th Conf. Radar Meteor.*, Boston, Mass., 2009. Am. Meteorol. Soc.

[2] Joachim Reuder, Pascal Brisset, Marius Jonassen, Martin Müller, and Sthephanie Meyer. The Small Unmanned Meteorological Observer SUMO: A

new tool for atmospheric boundary layer research. *Meteorol. Z.*, 18:141–147, 2009.

[3] T. G. Konrad, M. L. Hill, R. R. Rowland, and J. H. Meyer. A small, radio-controlled aircraft as a platform for meteorological sensors. *Appl. Phys. Lab. Tech. Digest*, 10:11–19, 1970.

[4] Thomas Spiess, Jens Bange, Marco Buschmann, and Peter Vörsmann. First application of the meteorological Mini-UAV 'M2AV'. *Meteorol. Z.*, 16:159–169, 2007.

[5] Ma Shuqing, Chen Hongbin, Wang Gai, Pan Yi, and Li Qiang. A miniature robotic plane meteorological sounding system. *Adv. Atmos. Sci.*, 21(6):890–896, 2004.

[6] G. J. Holland, P. J. Webster adn J. A. Curry, G. Tyrell, D. Gauntlett, G. Brett, J. Becker, R. Hoag, and W. Vaglienti. The aerosonde robotic aircraft: A new paradigm for environmental observations. *Bull. Amer. Meteorol. Soc.*, 82:889–901, 2001.

[7] Joseph Egger, Sapta Bajrachaya, Richard Heinrich, Philip Kolb, Stephan Lämmlein, Mario Mech, Joachim Reuder, Wolfgang Schäper, Pancha Shakya, Jan Schween, and Hilbert Wendt. Diurnal winds in the Himalayan Kali Gandaki Valley. Part III: Remotely piloted aircraft soundings. *Mon. Wea. Rev.*, 130:2042–2058, 2002.

[8] Joseph Egger, Luis Blacutt, Flavio Ghezzi, Richard Heinrich, Philip Kolb, Stephan Lämmlein, Martin Leeb, Stephanie Mayer, Eduardo Palenque, Joachim Reuder, Wolfgang Schäper, Jan Schween, Rene Torrez, and Francesco Zaratti. Diurnal circulation of the Bolivian Altiplano. Part I: Observations. *Mon. Wea. Rev.*, 133:911–924, 2005.

[9] Pascal Brisset, Antoine Drouin, Michel Gorraz, Pierre-Selim Huard, and Jeremy Tyler. The Paparazzi solution. available from www.recherche.enac.fr as mav06_paparazzi.pdf, 2006.

[10] Timothy Bonin, Brett Zielke, Wascar Bocangel, Wayne Shalamunenc, and Phillip Chilson. An analysis of wind retrieval algorithms for small unmanned aerial systems. In *Proc 91st AMS Ann. Conf.* Amer. Meteorol. Soc., 2011.

[11] R. M. Banta, R. K. Newsom, J. K. Lundquist, Y. L. Pichugina, R. L. Coulter, and L. Mahrt. Nocturnal low-level jet characteristics over Kansas during CASES-99. *Boundary-Layer Meteorol.*, 105:221–252, 2002.

[12] Robert M. Banta. Stable-boundary-layer regimes from the perspective of the low-level jet. *Acta Geophysica*, 56(1):58–87, 2008.

[13] T. E. VanZandt, T. L. Green, K. S. Gage, and W. L. Clark. Vertical profiles of refractivity turbulence structure constant: Comparison of observations by the Sunset Radar with a new theoretical model. *Radio Sci.*, 13(5):819–829, 1978.

[14] K. S. Gage and B. B. Balsley. On the scattering and reflection mechanisms contributing to clear air radar echoes from the troposphere, stratosphere, and mesosphere. *Radio Sci.*, 15(2):243–257, 1980.

[15] D. Hooper, J. Arvelius, and K. Stebel. Retrieval of atmospheric static stability from MST radar returns. *Ann. Geophys.*, 22:3781–3788, 2004.

[16] V. I. Tatarskii. *Wave Propagation in a Turbulent Medium*. McGraw-Hill, New York, 1961.

[17] Hans Ottersten. Mean vertical gradient of potential refractive index in turbulent mixing and radar detection of CAT. *Radio Sci.*, 4(12):1247–1249, 1969.

[18] K. S. Gage and J. L. Green. Evidence for specular reflection from monostatic VHF radar observations of the stratosphere. *Radio Sci.*, 13:991–1001, 1978.

[19] K. S. Gage, B. B. Balsley, and J. L. Green. Fresnel scattering model for the specular echoes observed by VHF radar. *Radio Sci.*, 16(6):1447–1453, 1981.

[20] K. S. Gage, W. L. Ecklund, and B. B. Balsley. A modified Fresnel scattering model for the parameterization of Fresnel returns. *Radio Sci.*, 20(6):1493–1501, 1985.

[21] Sheila Kirkwood, Maria Mihailikova, Daria Mikhaylova, Ingemar Wolf, and Phillip Chilson. Independent calibration of radar reflectivities using radiosondes: Applications to ESRAD. In *Proc 20th ESA Symposium on European Rocket and Balloon Programmes and Related Research*. European Space Agency, 2011.

[22] W. K. Hocking, R. Rüster, and P. Czechowsky. Absolute reflectivities and aspect sensitivities of VHF radio wave scatterers measured with the SOUSY radar. *J. Atmos. Terr. Phys.*, 48(2):131–144, 1986.

[23] S. Kirkwood, E. Belova, K. Satheesan, T. Narayana Rao, T. Rajendra Prasad, and S. Satheesh Kumar. Fresnel scatter revisited - comparison of 50 MHz radar and radiosondes in the Arctic, the tropics and Antarctica. *Ann. Geophys.*, 28:1993–2005, 2010.

[24] B. B. Balsley and K. S. Gate. The MST radar technique: Potential for middle atmospheric studies. *Pure Appl Geophys*, 18(1):452–493, 1980.

[25] Kenneth S. Gage. Radar observations of the free atmosphere: Structure and dynamics. In David Atlas, editor, *Radar in Meteorology*, pages 534–565. Am. Meteorol. Soc., Boston, Mass., 1990.

[26] Stephanie Mayer, Anne Sandvik, Marius O. Jonassen, and Joachim Reuder. Atmospheric profiling with the UAS SUMO: a new perspective for the evaluation of fine-scale atmospheric models. *Meteorol. Atmos. Phys.*, pages DOI 10.1007/s00703–010–0063–2, 2011.

[27] Joachim Reuder, Markus Ablinger, Hálfdán Ágústsson, Pascal Brisset, Sveinn Brynjólfsson, Markus Garhammer, Tómas Jóhannesson, Marius O. Jonassen, Rafael Kühnel, Stephan Lämmlein, Tor de Lange, Christian Lindenberg, Sylvie Malardel, Stephanie Mayer, Martin Müller, Haraldur Ólafsson, Ólafur Rögnvaldsson, Wolfgang Schäper, Thomas Spengler, Günther Zängl, and Joseph Egger. FLOHOF 2007: an overview of the mesoscale meteorological field campaign at Hofsjökull, Central Iceland. *Meteorol. Atmos. Phys.*, pages DOI: 10.1007/s00703–010–0118–4, 2011.